

Maritime surveillance radar

Part 2: Detection performance prediction in sea clutter

S. Watts, MA, MSc, PhD, CEng, MIEE
C.J. Baker, BSc, PhD
K.D. Ward, MA, PhD, CEng, MIEE

Indexing terms: Radar, Maritime surveillance, Detection, Clutter

Abstract: Techniques for detection performance prediction for maritime surveillance radars are described, with particular emphasis on the use of the compound K-distribution model for radar sea clutter. The paper first briefly reviews the analytical methods for deriving theoretical detection performance limits using compound models for both clutter and targets. Next, it is shown how the clutter environment is modelled for radar design evaluation, and methods whereby the radar may adapt to this changing environment for optimum target detection performance are described. This is followed by a description of a new method for performance prediction for a cell-averaging CFAR in real clutter, using recorded clutter signals but avoiding lengthy computer simulations. Finally, possible future developments of maritime surveillance radars are discussed.

1 Introduction

Part 1 of this paper [1] describes recent developments which have been made in the understanding and modelling of radar sea clutter. Particular emphasis is placed on the use of a compound form of the K-distribution for describing the amplitude characteristics of the clutter. The purpose of developing this model has not only been to provide a better descriptor of the clutter itself, but also for the design and assessment of improved target detection techniques.

In this paper, it is shown how the clutter models can be incorporated with target models to derive detection performance limits. Further, it is shown how the model can be exploited to investigate the performance of particular signal-processing techniques in a real clutter environment.

Section 2 of the paper describes a generalised approach to theoretical performance prediction based on the standard concepts of optimum threshold settings to achieve required false alarm rates.

Section 3 describes the modelling of the sea clutter

environment and its impact on the design of practical detection signal processing. This is extended to show how the compound K-distribution clutter model can be used to evaluate the detection performance of a cell-averaging CFAR detector using real clutter recordings as a data input.

Finally, Section 4 discusses areas where further improvements in detection signal processing may be expected.

2 Theoretical system performance prediction

The significant improvements in understanding and accuracy of performance evaluation which are achieved through the use of the compound K-distribution model are directly attributable to its compound nature. If the radar detection is based only on the fixed thresholding of a single variate (i.e. a single radar return), then performances can be predicted using a knowledge of the target and clutter probability density functions (PDFs) alone.

If, however, the radar processing involves the use of more than one variate, then the correlation properties of the target and clutter become important. This is so, for example, if the threshold fluctuates because it is derived from other range samples or if many pulse returns are averaged before (or after) thresholding. In these cases, the use of the compound form of the K-distribution provides a more accurate assessment of performance than a model based only on an overall PDF, since it allows correlation properties of the clutter to be accounted for. The target itself may have a PDF and correlation properties which can also be modelled by a compound distribution and this can be combined with the clutter model to produce more accurate detection performance predictions.

2.1 Detection prediction using compound distributions

A generalised approach to detection performance prediction is described here, followed by some examples.

The PDF of clutter can be written, in its compound form, as

$$p(x) = \int_0^{\infty} p(y)p(x|y) dy \quad (1)$$

For the compound K-distribution model $p(y)$ is the PDF of the local clutter power y , which is gamma distributed, with shape parameter ν and a scale parameter c :

$$p(y) = \frac{c^{2\nu} y^{\nu-1}}{\Gamma(\nu)} \exp(-c^2 y) \quad 0 \leq y \leq \infty \quad (2)$$

Paper 7151F (E15), first received 12th May 1989 and in revised form 2nd January 1990

© Controller, Her Majesty's Stationary Office, 1990

Dr. Watts is with THORN EMI Electronics Ltd., 248 Blyth Road, Hayes, Middlesex UB3 1HR, United Kingdom

Dr. Baker and Dr. Ward are at the Royal Signals and Radar Establishment, St. Andrew's Road, Malvern, Worcs. WR14 3PS, United Kingdom

and $p(x|y)$ is the PDF of the clutter amplitude for a given value of the local mean y . This is a Rayleigh distribution of mean power y :

$$p(x|y) = \frac{2x}{y} \exp\left(-\frac{x^2}{y}\right) \quad 0 \leq x \leq \infty \quad (3)$$

A case of general interest is when a detection threshold is set following the integration of several pulse returns. Often, the Rayleigh (or 'speckle') component of the clutter may be decorrelated from pulse to pulse (e.g. through the use of frequency agility) whilst the local mean power will remain approximately constant over the integration period. The local mean clutter power may vary spatially or, say, from scan-to-scan in an area surveillance radar.

Following the analogue integration of n pulse returns in these circumstances, the speckle component will have a modified PDF given by an n -fold convolution of $p(x|y)$, described here as $f_n\{p(x|y)\}$.

The probability of false alarm P_{fa} for a threshold level t is then given by

$$P_{fa} = \int_0^\infty p(y) \int_t^\infty f_n\{p(x|y)\} dx dy \quad (4)$$

The presence of a target will modify the returns to give an overall PDF of target plus clutter of $p(x; a)$, where the target has an amplitude a .

Considering first the simple case of a nonfading target with a fixed amplitude a , the probability of detection following the analogue integration of n pulses will be

$$P_d = \int_0^\infty p(y) \int_t^\infty f_n\{p(x; a|y)\} dx dy \quad (5)$$

A more general expression for P_{fa} and P_d can be given as

$$P_n(t; a) = \int_0^\infty p(y) P_n(t; a|y) dy \quad (6)$$

where $P_n(t; a|y)$ is the probability of detection for a known target amplitude a (or probability of false alarm when $a = 0$) in clutter for a given value of y , following the integration of n returns.

For a fluctuating target it is necessary to define whether the fluctuations are independent from pulse to pulse ('fast' fluctuations, as in Swerling cases 2 and 4, for example) or from scan to scan ('slow' fluctuations, as in Swerling cases 1 and 3).

For scan-to-scan fluctuations eqn. 6 becomes

$$P_n(t; \bar{a}) = \int_0^\infty \int_0^\infty p(a; \bar{a}) p(y) P_n(t; a|y) da dy \quad (7)$$

where \bar{a} is the average target amplitude and $p(a; \bar{a})$ is the PDF of the target amplitude.

For pulse-to-pulse fluctuations the expression for $P_n(t; a|y)$ will be modified so that now

$$P_n(t; \bar{a}) = \int_0^\infty p(y) \int_t^\infty f_n\left\{ \int_0^\infty p(a; \bar{a}) p(x; a|y) da \right\} dx dy \quad (8)$$

As another example, the targets may comprise both slow and fast fluctuating terms. In this case, the target PDF could be split into a compound form:

$$p(a; \bar{a}) = \int_0^\infty p(b; \bar{a}) p(a|b) db$$

where b is a measure of the slow fluctuating component. The detection performance of a fixed threshold might

now be described by

$$P_n(t; \bar{a}) = \int_0^\infty \int_0^\infty \int_t^\infty p(b; \bar{a}) p(y) \times f_n\left\{ \int_0^\infty p(a|b) p(x; a|y) da \right\} dx db dy \quad (9)$$

There is a further underlying assumption in the form of eqn. 9 which is that the target and clutter fading mechanisms are independent of each other. More complex interactions can readily be modelled, using similar techniques to those described above. In each case it is necessary to carefully analyse the various components of each model to establish their relationships with one another and their pulse-to-pulse fading characteristics. A number of specific examples are described in detail here and elsewhere. In Reference 2 (and here in Section 2.2) it is shown how multipath reflection interference can be incorporated. Reference 3 describes the addition of thermal noise where different approaches are needed, dependent not only on the different target models but also on whether or not the clutter speckle decorrelates from pulse to pulse with the noise. In References 4 and 6 it is shown how the detection performance of binary integrators can be derived.

So far, the derivations given here have assumed a fixed threshold for detection. In many cases the threshold may try to adapt to the local clutter mean level y , rather than assuming a fixed value determined by a false alarm rate averaged over all y . This may result in a considerable improvement in performance in some cases. A typical example would be a cell averaging CFAR receiver (e.g. Reference 5). A limiting case occurs when the threshold is assumed to exactly adapt to the local mean level y and this is termed 'ideal CFAR'. The calculation of detection performance in this case is described in Reference 4.

The estimation of performance in the more practical case where the adaptation of the threshold is not exact is discussed in more detail in Section 3 of this paper.

2.2 Example of performance prediction — target subject to multipath reflection interference

In this section we extend the analysis presented in Reference 2 of single-hit detection of a point target in the presence of multipath reflection interference and K-distributed sea clutter, to cover pulse-to-pulse integration. The radar signal at the target is modelled as the vector sum of a steady amplitude A , which is due to the interference between the direct illumination, a coherent sea reflection and a Gaussian noise-like term (with a standard deviation σ_n of the inphase and quadrature components) due to incoherent sea reflection. This gives rise to a target return amplitude having a Rice-squared (RS) distribution. As shown in Part 1 of this paper [1], A and σ_n depend upon the multipath geometry and the sea surface statistics. For given values of A and σ_n , the target return is assumed to be independent from pulse to pulse, which leads to the RS distribution being substituted for $p(a; \bar{a})$ in eqn. 8. For K-distributed sea clutter the term $p(x; a|y)$ in eqn. 8 has a Rice distribution, and $p(y)$ has a gamma distribution. (The equivalent analysis for single pulse detection is given in Reference 2.)

Fig. 1 shows performance results for detection following a ten-pulse binary integration, with a 6/10 threshold [4]. Various degrees of multipath interference are imposed on the target using the ratio A^2/σ_n^2 as a parameter, since it is a measure of the spread of the RS distribution, normalised to the target power. (If the target or

radar were to move during detection assessment, the parameter A^2/σ_n^2 would fluctuate slowly. This could be incorporated in the analysis by making a suitable substi-

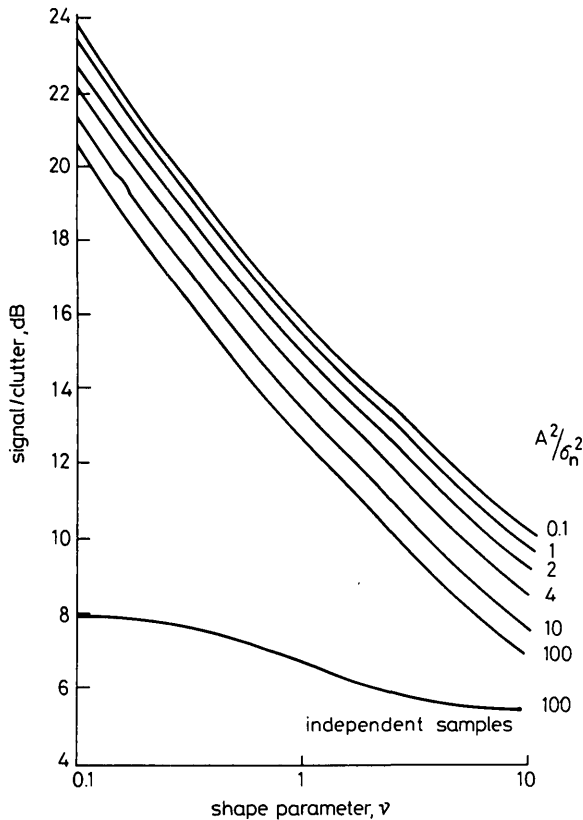


Fig. 1 Detection curves for nonfading target in K-distribution clutter with shape parameter ν , following 10-pulse binary integration (6/10 second threshold), for varying degrees of multipath interference

$P_d = 50\%$, $P_{fa} = 10^{-6}$

tution for $p(b; \bar{a})$ in eqn. 9). The figure shows that for a given target power, the effect of incoherent multipath fluctuations may reduce detection by up to 3 dB, irrespective of clutter statistics. Relating this to surface roughness is difficult to generalise, since both A and σ_n (and in consequence the target power) are a function of surface roughness, and A is also a function of position in the multipath fringe pattern. However, it is clear that the incorporation of multipath fluctuations in performance assessment is important.

Also included in Fig. 1 is a plot indicating the effect, for this type of target fluctuation, of ignoring the pulse-to-pulse correlation characteristics of the clutter. This demonstrates the point, made in Reference 6, that the compound correlated nature of the clutter is more important than the amplitude statistics. Thus the effect on target detection of changing from Gaussian statistics to a K-distribution with $\nu = 0.1$ is less than 3 dB (if pulse-to-pulse independence is assumed), whilst the real effect (calculated by using the compound K-distribution model) is a 12 dB degradation. It highlights the importance of using the compound form of the K-distribution, and illustrates the fact that simply taking an arbitrary distribution that only describes the amplitude properties of the sea echo is insufficient and will lead to over optimistic prediction of radar system performance when pulse-to-pulse integration is exploited in the signal processing.

3 Evaluation of practical detection techniques

3.1 Environment

The mathematical modelling techniques described in Section 2 provide the means for assessing the ideal per-

formance limits when the target and clutter characteristics are known. In practice the various shape and scale parameters of the amplitude distributions of targets and clutter will not be known *a priori* and a radar must adapt its processing to set the detection threshold at an appropriate level for the conditions actually encountered.

Before addressing the techniques which might be used to adapt the radar detection thresholds, it is necessary for the radar designer to be able to predict the range of conditions likely to be encountered, their dependence on various radar systems parameters and their likely rate of change, both temporally and spatially.

A number of empirical models for the shape and scale parameters of the distribution of the clutter envelope are available to assist the designer. These include models for clutter reflectivity, σ^0 , and the K-distribution shape parameter ν . The importance of these models is to provide guidance on the range of values likely to be encountered rather than providing any precise insight into the various parametric dependencies. The scale of the clutter returns can be estimated from a knowledge of the clutter reflectivity σ^0 . Many measurements of σ^0 have been published in the literature [7, 8] and several useful empirical models are available [9, 10] relating typical values of σ^0 to wind speed, wind direction, grazing angle, radar frequency and polarisation. Wind speed is often interpreted in terms of sea state or wave height, although it is local wind speed which appears to be the dominant factor in determining σ^0 , not the prevailing wave height. This is particularly likely to be so when there is a strong underlying sea swell resulting from wind-driven waves generated elsewhere. On the other hand, the sea swell is an important factor determining the shape of the clutter amplitude distribution. Empirical models for the K-distribution shape parameter ν are described in Reference 1, relating ν to grazing angle, across-range resolution, swell direction and radar polarisation. The empirical models of ν given in Reference 1 are strictly only for radar operating in I-band and for a single range resolution of about 4 m. As an initial guide to the range of values expected, the relationship between ν and range resolution can be considered as scaling in the same manner as between ν and the across-range resolution. However, the precise relationship is normally more complex and depends on the relative scaling of the radar pulse length and the spatial correlation of the clutter returns which will in turn often be determined by the sea swell wavelength. Further discussion of this can be found in Reference 11.

Using these empirical models for σ^0 and ν , pictures of the typical clutter environment can be developed as illustrated in Figs. 2 and 3. Fig. 2 shows the predicted signal

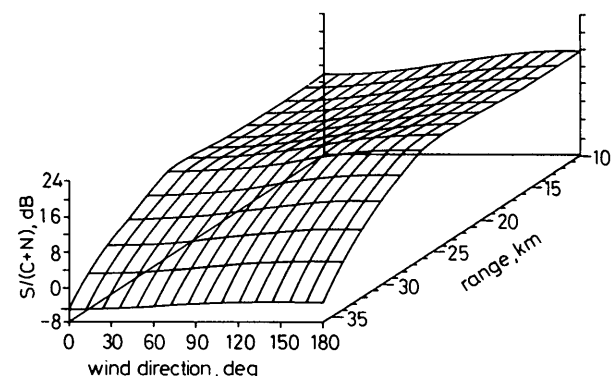


Fig. 2 Example of variation of signal to clutter-plus-noise ratio as function of wind direction and radar range

to clutter-plus-noise ratio $S/(C + N)$ for an example I-band radar, as a function of range to a target and the wind direction. The target is assumed to be on the sea surface and the wind speed is 10 m/s. The radar is also

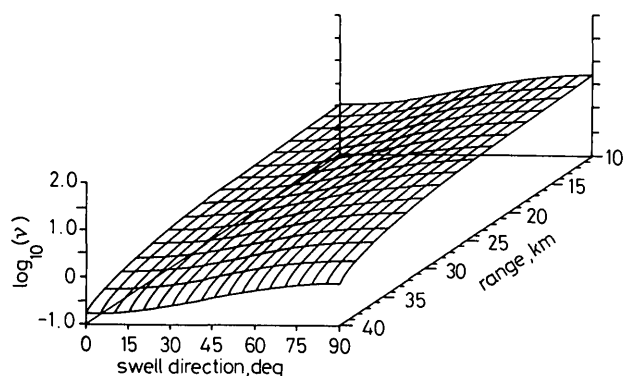


Fig. 3 Example of variation of K-distribution clutter shape parameter as function of sea-swell direction and radar range

assumed to have a 4 m range resolution and to be at a height of 100 m above the sea surface. Multipath effects on the target are not included. Although these figures are for a specific set of radar parameters, a number of typical features can be observed. The radar performance is clutter limited at short range and degrades initially with increasing range as the clutter return increases relative to the target. Thereafter $S/(C + N)$ increases again as σ_0 reduces with increasing range, until the performance becomes increasingly influenced by receiver thermal noise, resulting in a rapid reduction in performance towards maximum range. As well as this variation in range, there is a clear dependency on wind direction with $S/(C + N)$ varying over 5 dB between the up-wind and down-wind directions in the clutter limited region.

Fig. 3 shows a similar plot of the variation of K-distribution shape parameter for the clutter as a function of range and sea swell direction, for the same conditions as Fig. 2. It should be noted that there is generally no difference between the up-swell and down-swell values of ν observed and so Fig. 3 is only plotted over a 90° variation in swell direction. In this example the total spread of values shows ν potentially varying between values of about 5 and 0.5, although at ranges beyond about 30 km the performance will be increasingly dominated by receiver thermal noise in spite of the clutter becoming increasingly spiky. A more detailed discussion of the effects of combined clutter and noise can be found in Reference 3.

For single-pulse detection a useful approximation to detection performance can be achieved by assuming that the target is to be detected in clutter alone but with a modified value of ν given by

$$\nu_{eff} = \nu \left(1 + \frac{1}{CNR} \right)^2 \quad (10)$$

where CNR is the clutter-to-noise ratio [3].

As well as the overall amplitude characteristics specified by σ_0 and ν , it is necessary to have some insight into the likely spatial variation of the local clutter levels. This is particularly important for high resolution radars where the performance of adaptive thresholding techniques is being assessed. Some good examples of the range of conditions which can be found are given in References 1 and 11. Two specific examples of the variation of mean clutter level (γ in eqn. 2) as a function of range are given in Fig. 4. These will also be used in Section 3.2 for the discussion

on adaptive thresholding performance. These range profiles were taken from recordings obtained with an airborne I-band (8 GHz to 10 GHz) radar incorporating frequency agility, with an antenna beamwidth of 1.2° and a 28 ns pulse length. The envelope detected returns were averaged over several hundred pulses to remove the speckle component.

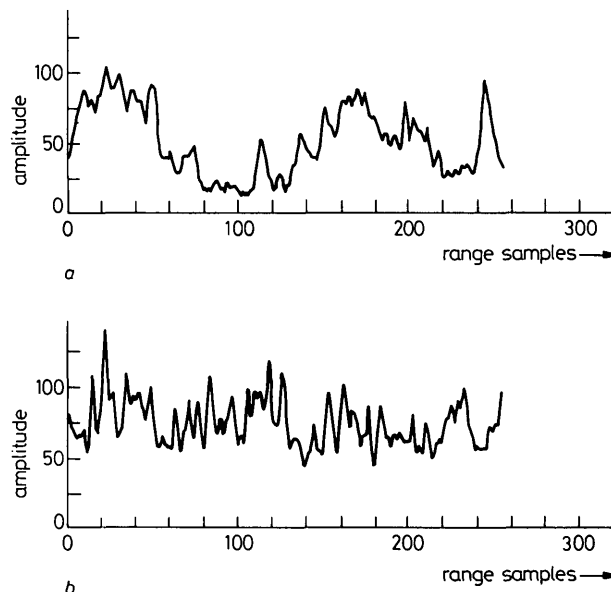


Fig. 4 Examples of radar range profiles of mean clutter envelope

One range sample interval = 2.6 m

a Down-swell direction, $\nu = 1.5$

b Across-swell direction, $\nu = 10$

The data in Fig. 4a was obtained with horizontal polarisation, looking down-swell in a sea-state 4 to 5, with a grazing angle of 0.9° and at a range of 34 km. The range profile shows a very strong periodicity with range which reflects the long wavelength sea swell which was observed at the time. This wide variation in local mean level is reflected in a shape parameter ν having a value of 1.5.

The data in Fig. 4b was collected under the same sea conditions but with vertical polarisation, a grazing angle of 4.3°, a range of 8 km and looking across-swell. This data exhibits a much smaller variation about its mean, as expected with the larger grazing angle and across-swell viewing direction.

This is reflected by a larger value of ν of about 10, indicating much more noise-like clutter returns when the speckle component is included.

These examples have been chosen to illustrate two very different clutter conditions which can be observed in the same area of sea. The optimum detection processing may be quite different for the two, as discussed in the next section.

3.2 Detection signal processing

The radar processor will be required to adapt its processing to match the clutter environment.

Nonparametric or distribution-free methods, such as those incorporating rank ordering techniques [12, 13] are not normally suitable for sea clutter since they require independent samples from pulse to pulse. As the clutter distributions are known to belong to the family of K-distributions, a better approach to CFAR design is to obtain estimates of the shape parameter ν and the scale of the returns and to use these to determine the threshold required. This type of approach is described in Reference 14 and a typical example of its use for Weibull clutter is given in Reference 15. Provided that the clutter local

mean level is fairly well decorrelated in range, suitable estimates of the distribution parameters should be obtainable using samples from a sliding window in range. In the limit, the performance achievable from such a CFAR processor should approach the fixed threshold results discussed in Section 2. Such a process can be described as CFAR in the sense that the overall P_{fa} is constant, but the P_{fa} will, in fact, have a spatial distribution dependent on the local value of mean clutter reflectivity. This may often reflect the best performance achievable, but clearly a 'fixed' threshold applied to the data in Fig. 4a would exhibit considerable spatial 'bunching' of false alarms.

For this type of clutter, it should be possible to adapt the threshold locally to follow more closely the mean level fluctuations. A well known approach is to use a cell-averaging CFAR [5], which with appropriate averaging length may well achieve better detection performance and control of false alarms than a fixed threshold (i.e. one that is determined only by the overall shape and scale of the clutter distribution). Such a detector is illustrated in Fig. 5, combined with a binary integrator.

ated with the sea swell) it may be possible to adapt to the local variations of mean level by using a cell-averaging length which is shorter than the sea swell wavelength. If the 'ideal CFAR' [4] conditions were to be achieved the value of β required would be independent of the distribution of the clutter local mean level. In practice some control of β is likely to be required but the range of values expected over a complete radar search area may be considerably reduced.

The precise interaction between a cell-averaging CFAR and the clutter returns will depend on the configuration of the CFAR system and the spatial correlation of the clutter. The use of shorter averaging lengths will enable the thresholds to follow more rapid spatial variations but will also introduce increased 'CFAR loss' due to fluctuations of the threshold induced by the speckle component of the clutter.

Clearly, the analytical prediction of performance of a short-length cell-averaging CFAR in spatially correlated clutter will be very difficult, particularly since no sufficiently accurate models of the spatial variations of the clutter returns currently exist. One method of assessing

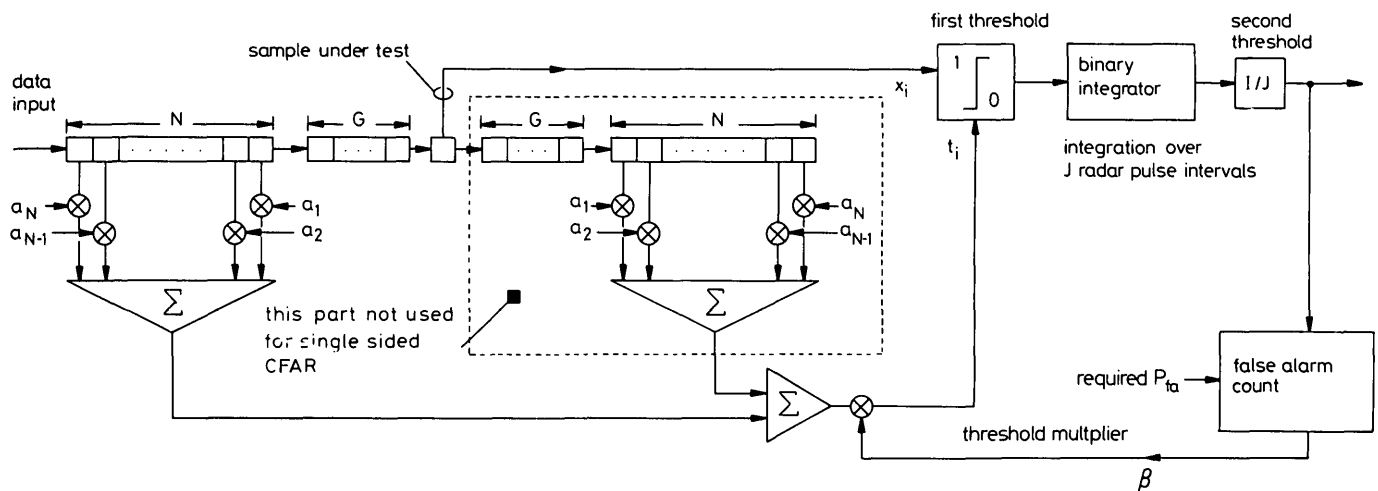


Fig. 5 Cell-averaging CFAR followed by binary integrator with feedback control of the first threshold multiplier β

Cell-averaging CFAR lengths in the text are given by N for single-sided CFARs and $2N$ for double-sided CFARs. The sample under test is separated from the CFAR filters by a gap of G samples and the transversal filter weights are given by $a_i, i = 1, \dots, N$.

If the cell-averaging length is very long, extending over several sea swell wavelengths, then the cell-averaging CFAR will provide an estimate of the overall mean clutter level. The false-alarm rate is determined by the multiplier β shown in Fig. 5 and the appropriate value for β is dependent on the clutter shape parameter.

If the shape parameter can be estimated as it varies over the area of operation of the radar, then the appropriate value of β could be calculated. Alternatively, a continuously adapting feedback system, such as described in Reference 16, could be used to maintain the desired false-alarm rate at the output of the detectors. On the assumption that β is estimated correctly, a cell-averaging CFAR detector with a sufficiently long averaging length should approach the performance of the ideal fixed threshold detector. In a typical application ν and hence β may vary quite widely. In the example of Fig. 3, ν varied between 0.5 and 5 and to maintain a constant false-alarm rate of 10^{-4} at the output of a binary integrator with a 6/10 second threshold would require values of β in the range 8 to 15 dB (ignoring any effects of thermal noise).

Reference to Fig. 4 suggests that when the returns show a strong periodic spatial variation (normally associ-

performance is to use recordings of real clutter as inputs to computer simulations of the signal processing. This is, however, extremely time consuming and it is difficult to achieve reliable estimates of very low false-alarm rates.

The use of the compound K-distribution model provides a means for a considerable simplification of the assessment of some signal-processing schemes using real clutter recordings as inputs, as described below.

3.3 Cell-averaging CFAR performance in real clutter

The performance of a cell-averaging CFAR followed by a binary integrator is illustrated here, as an example of the use of the compound K-distribution model for performance assessment of signal processing in real clutter. The basic detection system is shown in Fig. 5, although the dynamic performance of the feedback control of the threshold multiplier β will not be considered here.

The radar returns are first passed through a linear detector. This is followed by a single- or double-sided cell-averaging CFAR implemented in the form of a transversal filter with preset weights on each filter tap. This filter provides a weighted sum of the clutter range cells surrounding the cell under test. The output is multiplied

by a factor β and used to control the first threshold of a dual threshold binary integrator. The binary integrator operates over several radar pulses for each range cell. It is assumed that the radar employs pulse-to-pulse frequency agility to decorrelate the speckle component of the clutter.

One of the problems of a mathematical analysis of such a system is the description of the spatial variation of the clutter mean level. Rather than simply using raw clutter recordings in a full scale simulation, it is shown here how profile recordings of the mean level of real clutter (see Fig. 4, for example) can be used as the prime input, with a considerable saving in computer time.

A mathematical explanation of the method is given in the Appendix 7 but a summary of the techniques used is given here. It is assumed that mean level range profiles are provided in the form of linearly detected and sampled data with a sampling interval which is shorter than the range resolution of the radar pulse.

The first part of the method involves a computer simulation of the cell-averaging CFAR using the mean-level range profiles as input data. It is assumed that the real clutter range samples can be represented by Rayleigh variates with mean levels determined by the range profile. From this simulation it is possible to estimate the mean and variance of the cell-averaging CFAR filter output for each position in range. The mean-level estimate is simply the weighted sum of the range profile samples over the filter. The variance of the filter output is obtained from the weighted sum of the variances of the samples assuming them to be Rayleigh variates. Due allowances must be made in the calculation of variance for the fact that the data will in general be sampled more frequently than the range resolution of the radar pulse. This means that the Rayleigh component of successive range samples will be correlated.

After scaling with the required value of β we now have estimates of the mean and variance of the threshold as a function of range. The analysis which follows requires an estimate of the amplitude distribution of the threshold. For cell-averaging CFAR filters which use large numbers of independent range samples, this will be closely approximated by a Gaussian distribution using the central limit theorem. For shorter averaging lengths this approximation will not be so close but it has been found by comparison with direct simulation that even for very short lengths, equivalent to perhaps five independent samples, the approximation is adequate for the purposes of this evaluation.

3.3.1 Calculation of probability of false alarm P_{fa} : The cell-averaging CFAR threshold is assumed to have a Gaussian amplitude distribution with mean and variance which vary with range and with the chosen value of β .

For each range cell under test the probability of crossing the first threshold (i.e. the probability of false alarm) can now be calculated. The clutter return in the cell under test is assumed to have a Rayleigh distribution of known mean level and the probability of returns from this cell exceeding the threshold can be calculated analytically. It is necessary for ease of analysis that the distributions of the threshold and the cell under test are independent. This is achieved by leaving a gap between the cell under test and the nearest range samples used in the cell-averaging CFAR filter, to allow for the over-sampling in range of the data which occurs in practice.

For each range cell the probability of integrated returns exceeding the binary integrator second threshold

can also be calculated, assuming that independent samples of the threshold and cell return are obtained from one pulse to the next through the use of frequency agility.

The analysis is repeated for successive range cells providing values of P_{fa} at the first and second thresholds as a function of range for each value of β . The overall values of P_{fa} for each value of β are then obtained by averaging in range and over all the profiles used.

3.3.2 Calculation of probability of detection P_d : A similar procedure can be followed to estimate the probability of detection in each range cell. In this case, however, the cell under test is assumed to contain a target. In general, any target model can be used providing it is possible to generate the amplitude distribution of target and clutter combined. For the present investigation the initial emphasis has been on a nonfluctuating target which gives a Ricean distribution for the envelope of the returns. The target amplitude is chosen to give the required signal-to-clutter ratio when averaged over the complete range profile. For any particular range cell the amplitude distribution is then Ricean with parameters determined by the local signal-to-clutter ratio.

The P_d for each range cell can then be calculated for the required average signal-to-clutter ratios and with β set to give the required overall P_{fa} . The overall P_d is then obtained by averaging over all ranges and profiles used.

3.3.3 Performance results: As an example of the effectiveness of this technique, a number of results are shown here using the data illustrated in Fig. 4a. The detection is assumed to be a cell-averaging CFAR followed by a binary integrator with a 6/10 second threshold [4]. The probability of false alarm P_{fa} and probability of detection P_d are investigated as a function of β for a nonfading target.

Fig. 6 shows the expected P_{fa} in each range cell as a function of range for four different cell-averaging CFAR designs. Also shown is the mean level range profile used to obtain the results (the actual range interval used was longer, to allow for the settling time of the cell-averaging CFAR filters). A fixed value of β of 9 dB was used in each case.

The cell-averaging CFAR designs illustrated are for single- and double-sided averaging with either 10 or 50 samples averaged in total. The cell under test is assumed to be separated from the nearest of the cells used for averaging by one range sample up and down range.

It can be seen that the variation in P_{fa} with range is quite different for the different designs. The single-sided filter of length 50 range samples gives particularly large variations and the most uniform result is obtained with the double-sided filter of length 10 samples. These results are reflected in the values of β required to give particular values of overall P_{fa} when averaged over all range samples, as shown in Fig. 7.

The double-sided filters clearly perform better than the single-sided ones for this particular clutter. The 2 dB to 3 dB difference in the values of β required is directly reflected in the detection performance against a non-fading target, as shown in Fig. 8 for a P_{fa} of 10^{-4} . Also shown in Fig. 8 are the ideal detection curves calculated using the methods of Section 2 for a K-distribution with shape parameter ν of value 1.5. It can be seen that the cell-averaging CFAR curves follow the same trend as the

'ideal CFAR' detection, but with a CFAR loss which is about 4 dB for the double-sided filters and 7 dB for the single-sided filters.

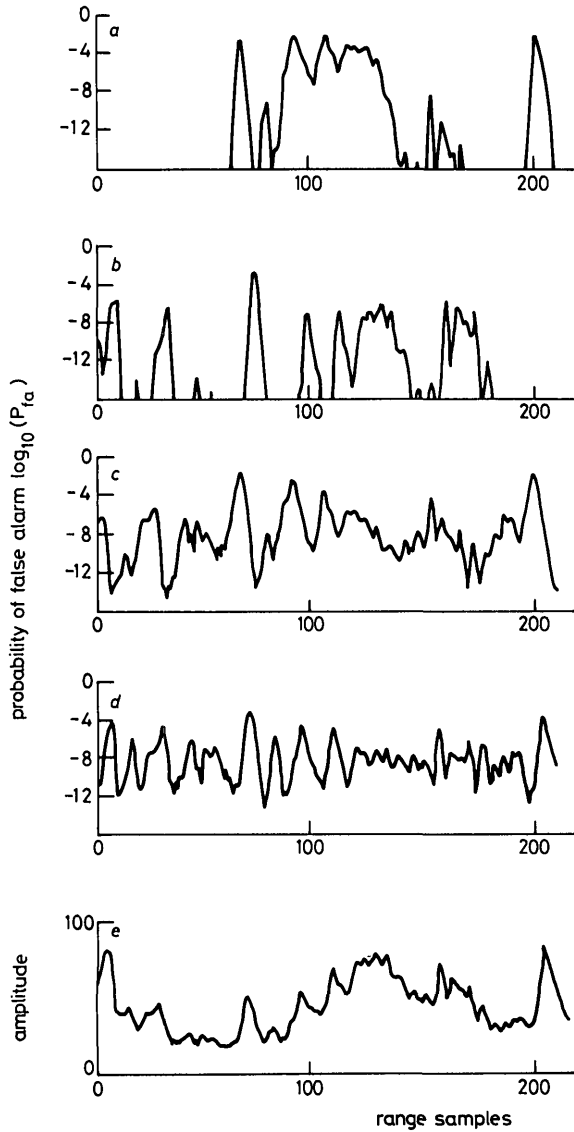


Fig. 6 Probability of false alarm as function of range for a number of cell-averaging CFAR configurations for the clutter illustrated in Fig. 4a

- a Cell-averaging length = 50; single-sided
- b Cell-averaging length = 50; double-sided
- c Cell-averaging length = 10; single-sided
- d Cell-averaging length = 10; double-sided
- e Range profile of mean clutter envelope

As a check of the method, direct simulation using raw (i.e. not averaged from pulse to pulse) clutter data from the same recordings was undertaken using artificially introduced nonfading targets. These results are also shown in Fig. 8 and are in good agreement with the semi-analytical results.

Exact equality of results is not expected due to the finite sample size used and also because targets were not simulated at all possible ranges in the raw clutter to save computer time. However, similar agreement between direct simulation and the analysis method was found over a variety of different clutter recordings which were also investigated, confirming not only the utility of the method but also the validity of the compound K-distribution model.

Finally, Fig. 9 shows the equivalent detection curves for the data illustrated in Fig. 4b. Here the spatial variation of the clutter is quite different and this is reflected in

the relative performance of the different cell-averaging CFAR systems. It can be seen that the best performance is now achieved by the longer double-sided filter, as would be expected in noise or Rayleigh distributed clutter. The theoretical detection curves for ν with a value

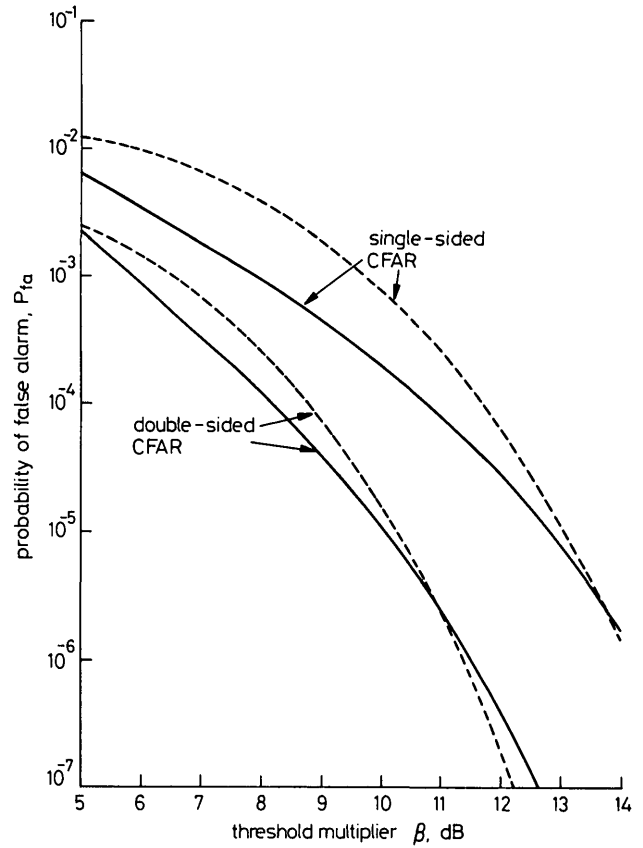


Fig. 7 Average probability of false alarm as function of threshold multiplier β for the clutter illustrated in Fig. 4a, for single- and double-sided cell-averaging CFAR systems followed by binary integrator with 6/10 second threshold

--- cell-averaging CFAR length 50; — cell-averaging CFAR length 10

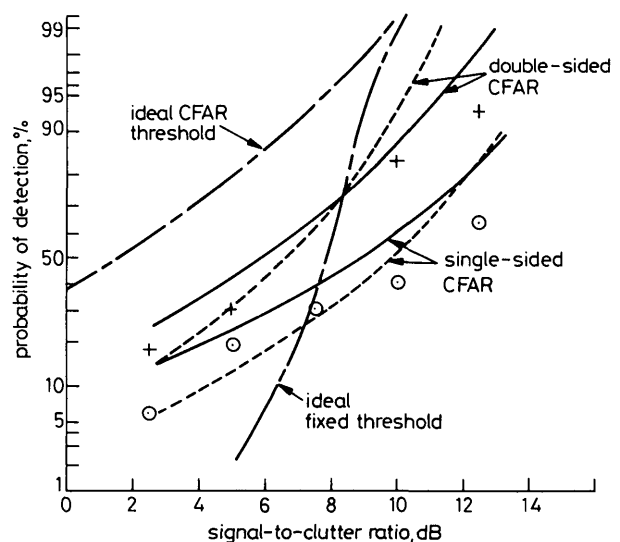


Fig. 8 Detection curves for nonfading target in the clutter illustrated in Fig. 4a for single- and double-sided cell-averaging CFAR systems followed by binary integrator with 6/10 second threshold and $P_{fa} = 10^{-4}$

Results obtained by combined analysis and simulation: — cell-averaging CFAR length 10; --- cell-averaging CFAR length 50
Results obtained by simulation using 'raw' clutter: + double-sided CFAR length 10; ○ single-sided CFAR length 50
Theoretical results: - - - ideal thresholds for $\nu = 1.5$

of 10 are also shown. The CFAR loss for the best performing cell-averaging CFAR is about 1.5 dB.

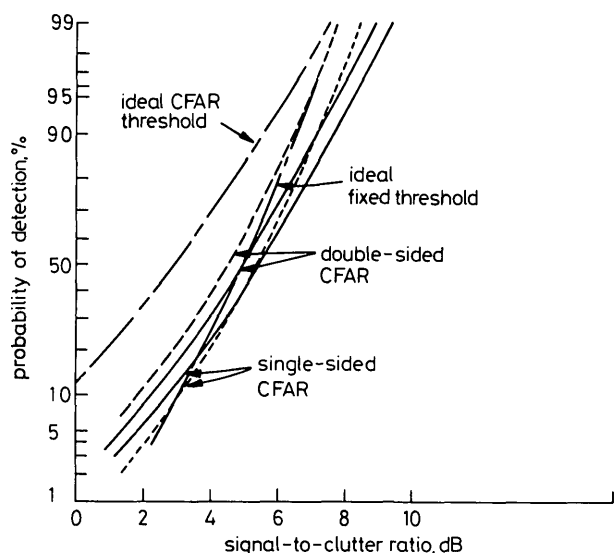


Fig. 9 Detection curves for nonfading target in the clutter illustrated in Fig. 4b for single- and double-sided cell-averaging CFAR systems followed by binary integrator with 6/10 second threshold and $P_{fa} = 10^{-4}$

Results obtained by combined analysis and simulation: —, cell-averaging CFAR length 10; - - - -, cell-averaging CFAR length 50
Theoretical results: - · - · -, ideal thresholds for $\nu = 10$

4 Future developments

The discussion in this paper has concentrated on the processing of envelope detected returns and this will continue to be an important mode of operation for high-resolution maritime surveillance radars. As has been demonstrated, clutter conditions can vary widely and are dependent on the radar parameters and on both the local wind and sea conditions.

An important aspect of future radars is likely to be their ability to adapt rapidly to provide the detection signal processing which is best matched to the local conditions. This may involve direct measurement of these conditions or indirect indications, such as the value of the threshold multiplier β required for a cell-averaging CFAR detector. When the clutter exhibits high spatial periodicity, one approach might be to adopt predictive techniques to improve the threshold setting. An example of this type of scheme applied to sea clutter is given in Reference 17, which describes the use of a lattice filtering technique.

The choice of the best signal-processing scheme should not be limited to a simple consideration of the expected value of probability of detection. It has been shown in this paper how the spatial distribution of false alarms may vary, dependent on the signal-processing scheme. Similar consideration must be given to the variation of probability of detection. For example, a fixed threshold may only detect a marginal target in regions of high clutter if the false-alarm rate is set at a low value, whilst a threshold which adapts to the local clutter level may provide its best detection in regions of low clutter for the same average false-alarm rate. The apparent target fading characteristics for these two detectors may be very different. However, the rather simplistic argument given here has so far ignored the characteristics of the target itself. Just as the improved understanding of clutter is providing considerable insight into the behaviour of signal-processing methods, so a similar understanding and modelling of targets will be essential to provide the

optimum detection techniques. Targets close to the sea surface will be influenced by such phenomena as multipath interference and shadowing by the sea waves. In some circumstances the return from the target may be actually dominated by the return from its wake or by wave splashing. In these conditions the target returns may appear to be correlated spatially and temporally with those of the clutter with obvious implications for any detection process.

The processing of only the envelope of returns from targets and clutter inevitably loses some of the information in the radar signal. Current research is investigating the spectra of coherent high-resolution clutter returns together with their full polarisation scattering matrix [1].

The spectra of clutter returns often have a spread which includes typical Doppler returns from surface targets. To make matters worse, it has been observed that the higher frequency components of the clutter spectra, which may coincide with typical target Doppler shifts, also have the 'spikiest' amplitude distributions. On the other hand, the spectra may also be rather asymmetric, resulting in some surface targets being detectable relatively free of clutter. The use of polarisation diversity is also likely to be important for the detection of marginal targets and clearly the characterisation of targets as well as clutter will be essential.

The discussion and results so far have implicitly been concentrated on the detection of small targets on the sea surface. Many targets will be range extensive relative to the range resolution of the radar and this involves further considerations of the appropriate detection techniques. A discussion of strategies for range extensive targets in uniform clutter can be found in Reference 18 and arguments of this sort can be extended to high-resolution sea clutter. With the advent of coherent radars for maritime surveillance it is likely that synthetic aperture radar (SAR) and inverse synthetic aperture radar (ISAR) techniques [19] will be increasingly used. SAR techniques can provide a high-resolution image of a ship. Significantly, the ship's wake is often very clearly imaged [20] and this may often be a more obviously detected signature than the ship itself.

ISAR methods are also becoming increasingly important and provide the opportunity for images of ships which closely resemble their optical profiles [19, 21].

5 Conclusions

This paper has shown how the recent advances in sea clutter modelling can be exploited in two ways: (a) to improve the understanding of the clutter environment in which a high-resolution maritime surveillance radar must operate and (b) to develop detection signal-processing techniques to meet the wide range of conditions encountered.

The maritime surveillance radars of the future are likely to be highly adaptive and able to employ a wide range of processing techniques to best fit the clutter and target characteristics that are encountered.

6 References

- WARD, K.D., BAKER, C.J., and WATTS, S.: 'Maritime surveillance radar. Part 1: Radar scattering from the sea surface', *IEE Proc. F, Radar & Signal Process.*, 1990, 137, (2), pp. 51-62
- TOUGH, R.J.A., BAKER, C.J., and PINK, J.M.: 'Radar performance in a maritime environment: single hit detection in the presence of multipath fading and non-rayleigh sea clutter', *IEE Proc. F, Radar & Signal Process.*, 1990, 137, (1), pp. 33-40

- 3 WATTS, S.: 'Radar detection prediction in K-distributed sea clutter and thermal noise', *IEEE Trans.*, 1987, **AES-23**, (1), pp. 40–45
- 4 WATTS, S.: 'Radar detection performance in sea clutter using the compound K-distribution model', *IEE Proc. Radar & Signal Process.*, 1985, **132**, pp. 613–620
- 5 FINN, M.M., and JOHNSON, R.S.: 'Adaptive detection mode with threshold control as a function of spatially sampled clutter-level estimates', *RCA Rev.*, 1968, **30**, pp. 414–465
- 6 WARD, K.D.: 'A radar sea clutter model and its application to performance assessment'. Radar-82, *IEE Conf. Publ. 216*, 1982, pp. 204–207
- 7 NATHANSON, F.E.: 'Radar design principles' (McGraw Hill, 1969)
- 8 LONG, M.W.: 'Radar reflectivity of the land and sea' (Lexington Books, 1980), pp. 77–79
- 9 HORST, M.M., DYER, F.B., and TULEY, M.T.: 'Radar sea clutter model'. Antennas and propagation Pt 2, *IEE Conf. Publ. 169*, November 1978, pp. 6–10
- 10 SITROP, H.: 'On sea clutter dependency on windspeed'. Radar 77, *IEE Conf. Publ. 155*, 1977, pp. 110–114
- 11 WATTS, S., and WARD, K.D.: 'Spatial correlation in K-distribution sea clutter', *IEE Proc. F, Radar & Signal Process.*, 1987, **134**, (6), pp. 526–532
- 12 HANSEN, V.G., and OLSEN, B.A.: 'Non-parametric radar extraction using a generalised sign test', *IEEE Trans.*, 1971, **AES-7**, (5), pp. 942–950
- 13 DILLARD, G.M., and ANTONIAK, C.E.: 'A practical distribution-free detection procedure for multiple range-bin radar', *IEEE Trans.*, 1970, **AES-6**, (5), pp. 629–635
- 14 HANSEN, V.G.: 'Constant false alarm rate processing in search radars', in 'Radar: present and future', *IEE Conf. Publ. 105*, 1973, pp. 325–332
- 15 GOLDSTEIN, G.B.: 'False alarm regulation in log-normal and Weibull clutter', *IEEE Trans.*, 1973, **AES-9**, (1), pp. 84–92
- 16 VOGEL, L.E., et al.: 'An examination of radar signal processing via non-parametric techniques'. Proc. IEEE 1975 Int. Radar Conf., pp. 533–537
- 17 DARWISH, H., and COOPER, D.C.: 'The log-lattice detector for radar targets in sea clutter'. IEE Colloquium Digest 1986/69, Discrimination and identification methods in radar and sonar systems, 6th May 1986, pp. 9.1–9.6
- 18 HUGHES, P.K.: 'A high-resolution radar detection strategy', *IEEE Trans.*, 1983, **AES-19**, (5), pp. 663–667
- 19 WEHNER, D.R.: 'High resolution radar' (Artech House, 1987)
- 20 ELDHUSET, K.: 'Automatic ship and ship wake detection in SAR images from coastal regions'. IGARSS'88, ESA SP-284, 3, August 1988, pp. 1529–1533
- 21 SMITH, J.M.: 'AN/APS-134(V) maritime surveillance radar'. Radar-82, *IEE Conf. Publ. 216*, October 1982, pp. 36–40

7 Appendix: Performance of a cell-averaging detector in real clutter

7.1 Basic definitions and assumptions

The signal processing architecture being analysed is shown in Fig. 5.

The data input to this analysis is assumed to be successive samples in range of the mean clutter envelope (i.e. a mean level range profile). These values are given by y_i , where $i = 1, 2, \dots$, denotes successive samples in range. It should be noted that, for analytical convenience, y is taken as representing the average of the clutter envelope and not the clutter power as shown in eqn. 2 of the paper.

It is assumed that individual radar returns from a particular range cell will be Rayleigh distributed about their mean level y_i . The use of frequency agility is assumed to provide independent Rayleigh samples from pulse to pulse.

The running average is performed over N samples. The analysis here assumes a single-sided cell-averaging CFAR but can be easily extended to the double-sided case.

Finally it is assumed that the threshold has a Gaussian amplitude distribution with mean and variance calculated from the input data and appropriate filter parameters.

7.2 Clutter amplitude distributions

The overall clutter distribution is assumed to be given by

$$p(x) = \int_0^{\infty} p(y)p(x|y) dy \quad (11)$$

where $p(y)$ is the distribution of the mean clutter level y , and $p(x|y)$ is the distribution of clutter about a given mean level y . It is assumed that $p(x|y)$ is Rayleigh distributed so that

$$p(x|y) = \frac{\pi x}{2y^2} \exp\left(\frac{-\pi x}{4y^2}\right) \quad 0 \leq x \leq \infty \quad (12)$$

Given a threshold value t , the probability of false alarm for this distribution is given by

$$P_{fa} = \exp\left(\frac{-\pi t^2}{4y^2}\right) \quad (13)$$

7.3 Threshold mean and variance

Successive values of the cell-averaging CFAR filter output are given by the weighted sum of N partially correlated Rayleigh variates. Given the mean clutter range profile y_i it is possible to obtain estimates of the mean and variance of the output at each position in range.

In general, successive values of the mean of the output are given by

$$\bar{r}_j = \left(\sum_{i=1}^N a_i y_{i+j}\right) \cdot \left(\sum_{i=1}^N a_i\right)^{-1} \quad (14)$$

where a_i , $i = 1, \dots, N$ are the filter weights. For simplicity we shall consider a single output r_m , where we arbitrarily set

$$j = 0 \quad \text{and} \quad \sum_{i=1}^N a_i = 1$$

so that now

$$\bar{r}_m = \sum_{i=1}^N a_i y_i \quad (15)$$

The threshold mean level is now simply obtained by multiplying by β so that

$$\bar{t} = \beta \sum_{i=1}^N a_i y_i \quad (16)$$

The threshold variance is found by considering the variance of the weighted sum of N partially correlated Rayleigh variates.

If we take N variates x_i , $i = 1, \dots, N$, with mean $\bar{x}_i = a_i y_i$ and variance

$$\text{var}(x_i) = a_i^2 \sigma_i^2 = a_i^2 y_i^2 \left(\frac{4}{\pi} - 1\right)$$

where σ_i^2 is the variance of a Rayleigh variate with mean y_i , then the variance of the filter output can be written as

$$\text{var}\left(\sum_{i=1}^N x_i\right) = \sum_{i=1}^N \text{var}(x_i) + 2 \sum_{j=1}^{N-1} \sum_{i=1}^{N-j} \text{cov}(x_i, x_{i+j}) \quad (17)$$

Now the covariance terms can be expressed as

$$\begin{aligned} \text{cov}(x_i, x_j) &= E\{(x_i - \bar{x}_i)(x_j - \bar{x}_j)\} \\ &= \rho_{ij} \sigma_i \sigma_j \end{aligned} \quad (18)$$

where ρ_{ij} is the correlation coefficient for x_i and x_j . It is assumed here that the appropriate correlation coefficient is determined by the radar pulse length and the sampling interval and that it is independent of the actual values of

x_i and x_j . We can then write

$$\text{cov}(x_i x_{i+k}) = \rho_k \sigma_i \sigma_{i+k} \quad (19)$$

For the data considered here the sampling interval is approximately half the pulse length so that it should be sufficient to use only the first two lags of the correlation coefficient, ρ_1 and ρ_2 . We can then write

$$\text{var} \left(\sum_{i=1}^N x_i \right) = \sum_{i=1}^N a_i^2 \sigma_i^2 + 2 \sum_{j=1}^2 \rho_j \sum_{i=1}^{N-j} a_i a_{i+j} \sigma_i \sigma_{i+j} \quad (20)$$

The variance of the filter output can now be expressed in terms of the mean levels of the input signals as

$$\text{var}(r_m) = \left(\frac{4}{\pi} - 1 \right) \left\{ \sum_{i=1}^N a_i^2 y_i^2 + 2 \sum_{j=1}^2 \rho_j \sum_{i=1}^{N-j} a_i a_{i+j} y_i y_{i+j} \right\} \quad (21)$$

The threshold variance is now given by

$$\text{var}(t) = \sigma_t^2 = \beta^2 \text{var}(r_m) \quad (22)$$

The probability distribution $p(t)$ of the threshold is assumed to be Gaussian so that

$$p(t) = \frac{1}{\sqrt{2\pi} \sigma_t} \exp \left(- \frac{(t - \bar{t})^2}{2\sigma_t^2} \right) \quad (23)$$

7.4 P_{fa} at the first threshold

The probability of false alarm is now calculated for each filter position over the range profile, assuming a Gaussian threshold.

Using eqns. 13 and 23 we can write, for any one filter position,

$$P_{fa}(\bar{t}, \sigma_t) = \int_0^\infty P_{fa}(t) p(t | \bar{t}, \sigma_t) dt \simeq \int_0^\infty \exp \left(\frac{-\pi t^2}{4y^2} \right) \frac{1}{\sqrt{2\pi} \sigma_t} \exp \left(- \frac{(t - \bar{t})^2}{2\sigma_t^2} \right) dt \quad (24)$$

The integration of the Gaussian distribution for $t < 0$ can be ignored for $t \gg \sigma_t$, which is normally the case. Indeed, the approximation will only be reasonable under these circumstances since t will never be negative in practice. Putting

$$\alpha = 1 + \frac{\sigma_t^2 \pi}{2y^2}$$

gives

$$P_{fa}(\bar{t}, \sigma_t) = \frac{1}{\sqrt{2\pi} \sigma_t} \exp \left\{ \frac{\bar{t}^2}{2\sigma_t^2} \left(\frac{1}{\alpha} - 1 \right) \right\} \times \int_0^\infty \exp \left\{ - \frac{\alpha}{2\sigma_t^2} \left(t - \frac{\bar{t}}{\alpha} \right)^2 \right\} dt \quad (25)$$

Provided $\bar{t}/\alpha \gg \sigma_t/\sqrt{\alpha}$ the integral can be performed over the limits $-\infty$ to ∞ without loss of accuracy giving

$$P_{fa}(\bar{t}, \sigma_t) = \frac{1}{\sqrt{\alpha}} \exp \left\{ - \frac{\bar{t}^2}{2\sigma_t^2} \left(\frac{1}{\alpha} - 1 \right) \right\} \quad (26)$$

The value of P_{fa} is calculated for each cell averager position over the range profile and then averaged to give the overall value of P_{fa} for that profile. As discussed earlier, P_{fa} is clearly also now available as a function of range along the profile.

It should also be noted that implicit in this analysis is the assumption that the threshold value t is not correlated with the Rayleigh component of the cell under test.

7.5 P_{fa} at the second threshold

The probability of false alarm at the second threshold (after the binary integrator) can be easily calculated from the value obtained at the first threshold for each filter position along the profile (see Reference 4 for further discussion on binary integration). It is assumed that the Rayleigh components of the clutter samples are independent from pulse to pulse either from the use of frequency agility or temporal decorrelation.